Chapter 5. Measurement of compressional wave properties

Techniques previously used in the literature to measure compressional wave velocity, attenuation coefficient and quality factor from transmission data general suffer from one of the following:

1. The assumption that spreading losses in the overlying water column and the sediment are the same.
2. An examination of the variability of the acoustic wave emitted by the source is not presented.
3. An examination of the repeatability of the coupling of the source and receiver transducers to the sediment is not presented.
4. A detailed analysis of intrinsic errors is not presented.
5. The assumption that attenuation coefficient is proportional to frequency in LSR techniques.

The techniques used in this project have been specifically designed to accommodate these issues. *Sections 4.2* and *4.3* have dealt with issues 1) and 2), whilst *Chapter 5* will discuss issues 3) to 5). In the remainder of this thesis compressional wave velocity, compressional wave attenuation coefficient and compressional wave quality factor will simply be referred to as velocity, attenuation coefficient and quality factor.

5.1. Pre-processing of acoustic data

For each location examined, five sets of signals were acquired for each S-R separation and central frequency used (*Section 4.4.1*). Each set of signals includes the *voltage output signal* sent to the source transducer and the signals detected by the two receivers. These signals were pre-processed in order to increase the signal-to-noise ratio (SNR) of the received signal, and so permit a more accurate examination of the directly transmitted pulse. As the velocity analysis incorporates a correlation between the *voltage output pulse* and the received signal, identical pre-processing steps were applied to both of these signals. The pre-processing incorporates two stages: filtering (*Section 5.1.1)* and stacking (*Section 5.1.2*).

5.1.1. Design and application of filters.

The first stage was to filter each shot individually. Care was taken to design filters that enhanced the pulse of interest while having a constant effect at each central frequency examined.

In order to design such filters it was necessary to examine the spectral content of typical received signals and *voltage output pulses*. *Figure 5.1* displays the spectrum of a typical *voltage output pulse*, which displays peak spectral amplitude at a generic central frequency f_c. A measure of the useful energy contained in the pulse E_T is obtained from

$$E_T = \frac{1}{\rho \cdot v} \int_{f_1}^{f_2} W(f)^2 \qquad 5.1,$$

where f_1 and f_2 represent the frequencies at which the spectral amplitude $W(f)$ reduces to 1 % of the peak spectral amplitude W_P, ρ represents density and v represents velocity (Medwin and Clay, 1998). The frequencies corresponding to 10 % of the peak value, denoted by f_+ and f_- respectively, were selected as initial estimates for filter cut-off points, as spectral amplitudes less than this were less robust to the presence of noise. The amount of "useful" energy retained within the 10 % limits E_{10} can be obtained from

$$E_{10} = \frac{1}{\rho \cdot v} \int_{f_-}^{f_+} W(f)^2 \qquad 5.2.$$

Hence the percentage of useful energy retained within the 10 % limits $\%E_{10}$ can be obtained from

$$\%E_{10} = 100 \cdot \frac{E_{10}}{E_T} \qquad 5.3.$$

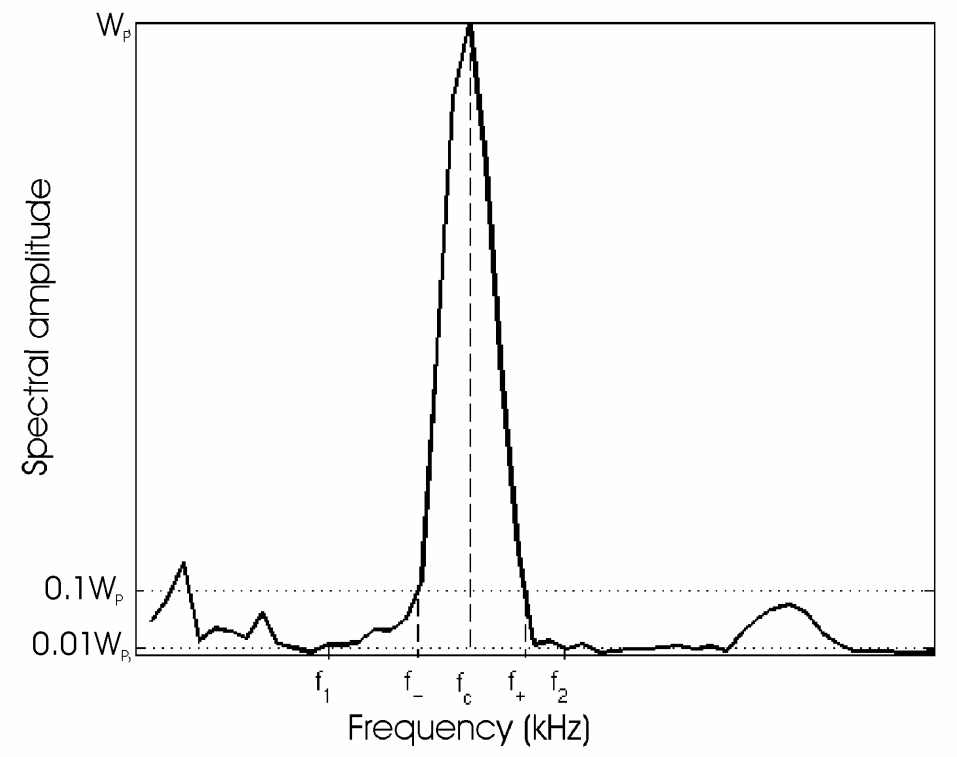

Figure 5.1. Diagrammatic representation of the amplitude spectrum of a typical voltage output pulse, which displays generic frequencies of f_1, f_2, f_-, f_+ and f_c.

In order to develop the optimum filters, a trial dataset was examined. This dataset included all received signals and *voltage output signals*, which correspond to *voltage input pulses* with central frequencies between 20 and 100 kHz in 10 kHz steps, from the following S-R separations and locations:

- Branksome 2, at a S-R separation of 3.22 m.
- Branksome 1, at a S-R separation of 2.57 m.
- Studland 4, at a S-R separation of 2.50 m.
- Mercury 2, at a S-R separation of 4.92 m.
- Needs Ore 1, at a S-R separation of 4.80 m.

The selection above spans the full range of sediment types examined and typical S-R separations used, while the frequencies selected effectively span the range of central frequencies used in the transmission experiments. The central frequencies of the *voltage input pulse*, *voltage output pulse* and received signals all vary from one another. The relationship between the central frequencies of the *voltage output pulse* f_o and the *voltage*

input pulse f_i is displayed in *Equation 4.3*. The relationship between the central frequencies of the received signal f_r and the *voltage input pulse* f_i is expressed as

$$f_r = 0.96 \cdot f_i + 0.62 \qquad 5.4.$$

For the trial dataset, the standard deviation in f_r was less than 3 % of the value of f_r predicted by *Equation 5.4*. For simplicity, the central frequencies discussed in the remainder of this *Chapter* will correspond to those of the *voltage input pulse*, with the actual central frequencies of *voltage output pulse* and received signals related to the stated frequency through *Equations 4.3* and *5.4* respectively.

Figure 5.2 displays the values of $\%E_{10}$ for the *voltage output signals* in the trial dataset. For all frequencies examined, the 10% limits retain over 94% of the useful energy, while from 30 to 90 kHz more than 97.5 % of the useful energy is retained. Though the $\%E_{10}$ should also be calculated for the received signals, the noisier nature of the received signal distorts spectral amplitudes that are less than 5% that of the peak amplitude (*Figure 5.3*), resulting in values of E_T, and so $\%E_{10}$, that are deemed unreliable. However, as the spectrum of the received signal within the 10% limits is simply a stretched version of the spectrum of the *voltage output signal* over these limits, it is assumed that a similar percentage of useful energy is retained for the received signal.

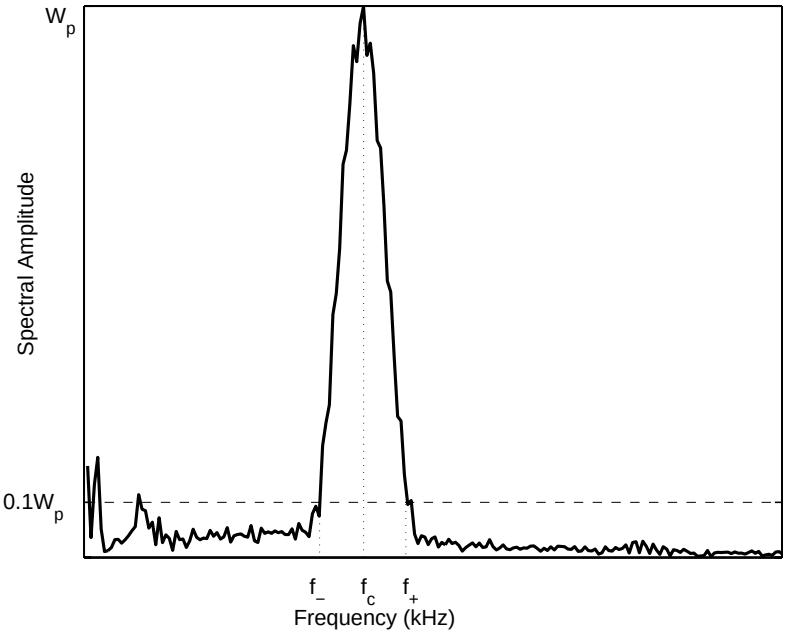

Figure 5.2. Diagrammatic representation of the spectrum of a typical received signal, which displays relative locations of generic frequencies f_+, f_- *and* f_c.

The spectra of the signals in the trial dataset were also examined to determine the frequencies at which dominant noise events occurred. At central frequencies of 20 kHz noise events occurred at frequencies of 35 kHz and greater. At central frequencies between 30 and 100 kHz, voltage output signals contained dominant noise at frequencies of less than 10 kHz and greater than 300 kHz, while received signals primarily contained noise at frequencies less than 20 kHz, with additional spikes at 40 kHz and 120 kHz.

The high percentage of useful energy retained by the 10% limits and the presence of noise outside these limits supports the selection of the 10% limits as acceptable initial estimates of cut-off points for the filter design.

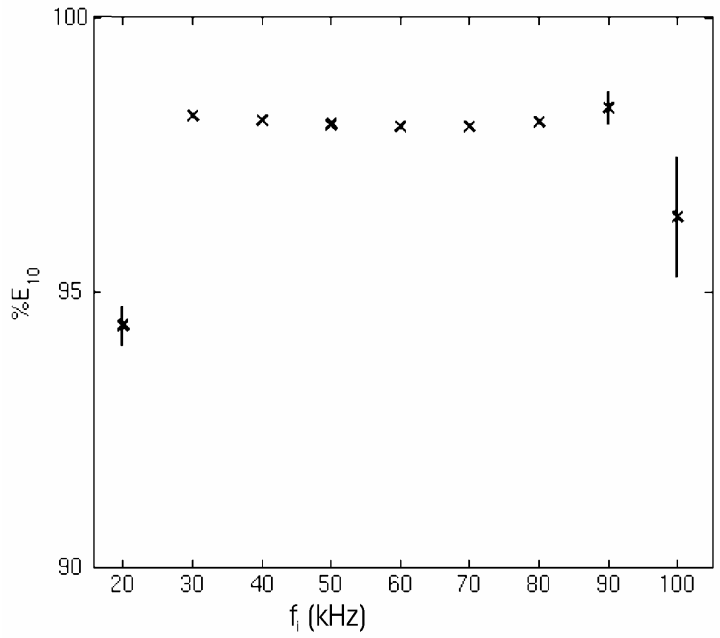

Figure 5.3. Percentage of "useful" energy retained by 10 % limits for voltage output signals from the trial dataset. Mean values are denoted by crosses, while vertical lines denote standard deviations.

In order to design universal filters which could be applied to all datasets examined, it was necessary to standardise the cut-off points. For each location and central frequency examined in the trial dataset the 10 % limits f_+ and f_- were re-expressed as the dimensionless positive L_+ and negative L_- limit parameters. These were defined for the *voltage output pulse* using

$$L_+ = \frac{(f_+ - f_o)}{B_o} \qquad 5.5,$$

$$L_{-} = \frac{(f_o - f_{-})}{B_o} \qquad 5.6,$$

where B_o represents the bandwidth of the *voltage output pulse*, which is obtained as described in *Section 4.2*. The positive and negative limit parameters of the received pulse were obtained from *Equations 5.5* and *5.6* by replacing f_o by f_r. It was chosen to express the limit parameters for both the voltage output and received pulses in terms of B_o owing to the more variable nature of the bandwidth of the received pulse.

The positive and negative limit parameters of the *voltage output signals* are displayed in *Figure 5.4*. Both L_+ and L_- are independent of central frequency, varying from 1.3 to 1.4 for L_+ and 1.2 to 1.35 for L_-, with standard deviations less than 0.1. *Figure 5.5* displays the same parameters for the received signals in the trial dataset. Both L_+ and L_- display mean values less than those for the *voltage output signal*. The larger standard deviations observed for the received signals (*i.e.* up to 0.4) are a consequence of the noisier, and so less reliable, nature of the received signals. Values of L_+ range from 0.9 to 1.05, while L_- is less than 1. For both the voltage output and received signals, L_+ is greater than L_-. Hence the selection of passband which extends from $f_c+1.5 \cdot B_o$ to $f_c-1.3 \cdot B_o$ will result in the inclusion of greater than 94 % of the useful energy for all signals and datasets. The filters used consisted of bandpass Butterworth filters with a pass-band ranging from $f_c+1.5 \cdot B_o$ to $f_c-1.3 \cdot B_o$, over which the filter response is flat to within 0.01 dB. The stop-band incorporated frequencies less than $f_c-2.6 \cdot B_o$ and greater than $f_c+3 \cdot B_o$, which were attenuated by greater than 100 dB with respect to the passband. This was the smallest stop-band which could be used, which allowed fluctuations in filter response across the pass-band to be kept less than 0.01 dB. Examples of the filter frequency responses corresponding to central frequencies of 20, 50 and 100 kHz, are displayed in *Figure 5.6*.

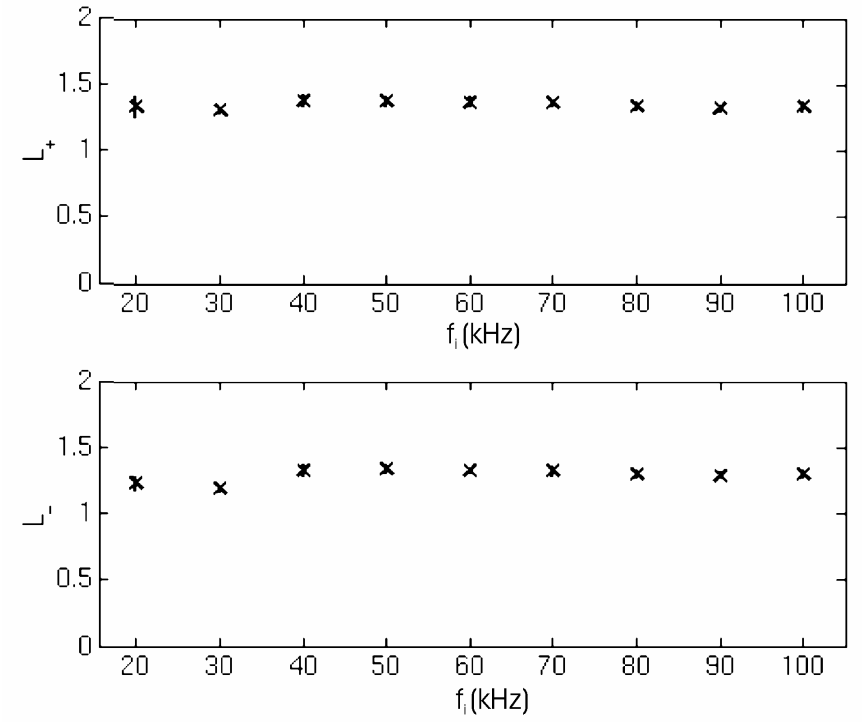

Figure 5.4. Positive and negative limit parameters, L_+ and L_-, for voltage output signals in trial dataset. Both mean values (crosses) and standard deviations (vertical lines) are displayed.

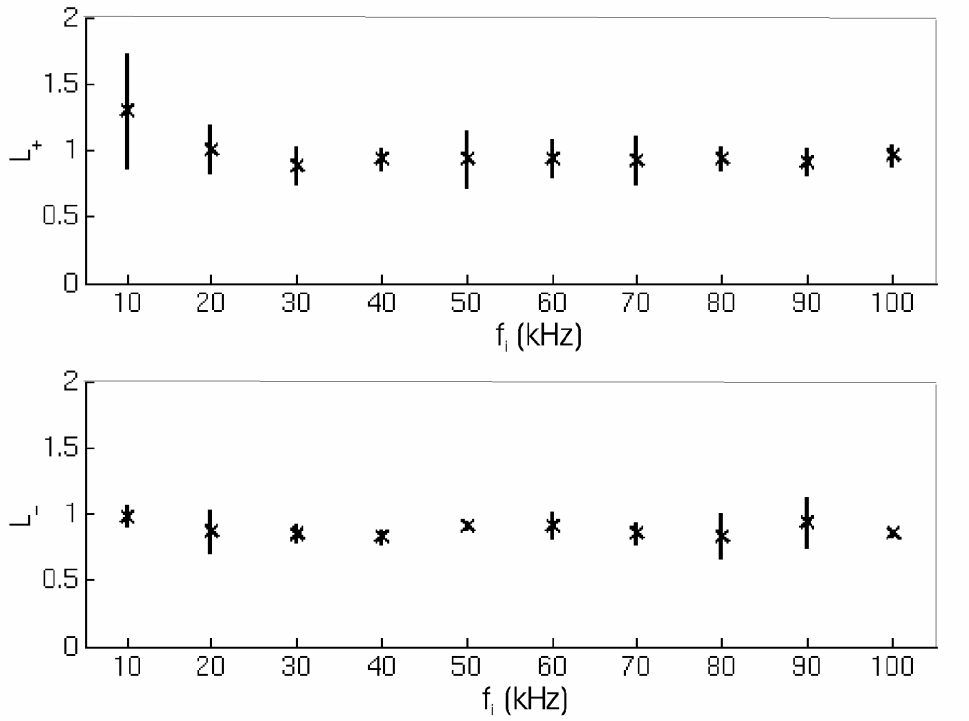

Figure 5.5. Positive and negative limit parameters, L_+ and L_-, for received signals in trial dataset. Both mean values (crosses) and standard deviations (vertical lines) are displayed.

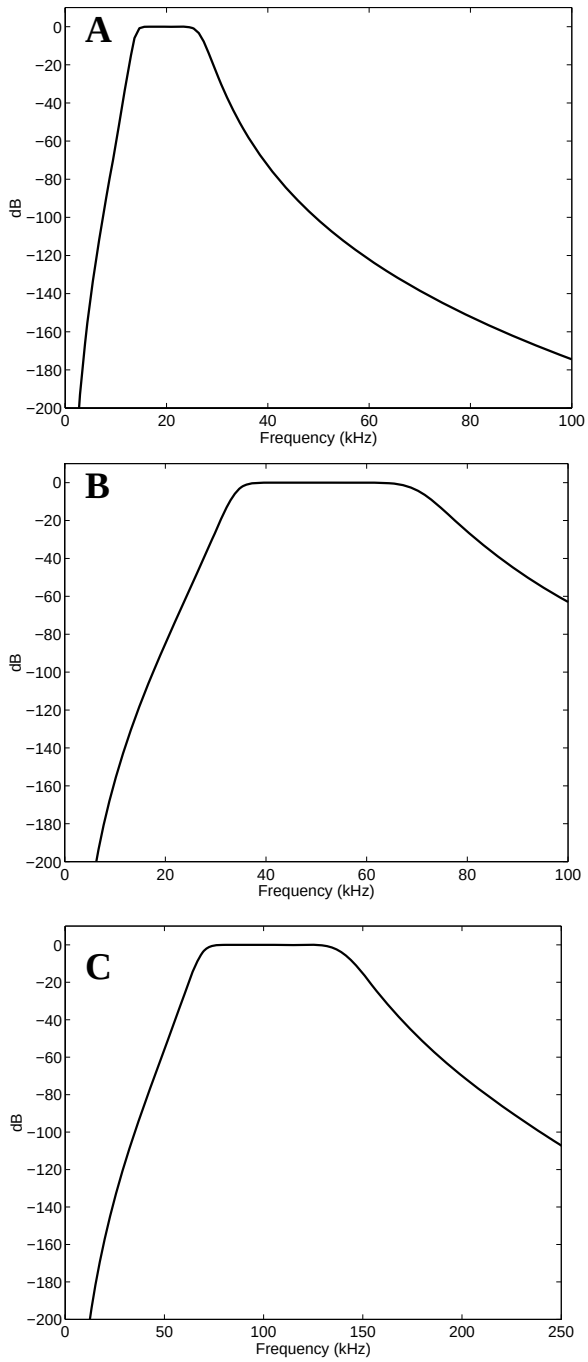

Figure 5.6. Squared filter frequency responses of typical Butterworth filters applied at central frequencies of 20 kHz (A), 50 kHz (B) and 100 kHz (C). Note the varying frequency scales used, which allow the necessary details of each filter to be clearly displayed.

These filters were applied to all *voltage output pulses* and received signals in a non-causal manner. This was achieved through the use of a filter operation which ensures

zero phase shift. Application of causal filters can shift certain frequency components and so alter pulse shape and result in anomalous arrival times (Yilmax, 1987).

In summary the resulting filters applied were designed in such a manner as to:

- Ensure maximum noise removal.
- Minimise the removal of "useful" energy.
- Retain a constant percentage of the "useful" energy across all central frequencies examined.

Hence any frequency-dependent variations observed in group velocity, attenuation coefficient and quality factor can be directly attributed to the sediment through which the compressional waves have propagated.

5.1.2. Stacking

The second stage of the pre-processing was to stack the filtered shots, using a median average. The use of a median, which selects the central value of a range of values, reduced the influence of random noise events. For received signals that displayed low SNRs, random interference events occasionally possessed amplitudes greater than that of the directly transmitted pulse and therefore could produce unreliable measurements of compressional wave properties. *Figure 5.7* compares the application of a mean and median stack to a typical received signal with a low SNR. The removal of random interference events by the median stack allows the directly transmitted signal, which occurs between 2.5 and 2.6 ms, to be more easily identified, while the envelope of the directly transmitted pulse is also improved.

The use of a median stack results in a SNR enhancement S_n given by

$$S_n = \sqrt{\frac{2N_S}{\pi}} \qquad 5.7,$$

where N_S is the number of shots stacked (Cramer, 1946). For the five shots collected within the fieldwork, *Section 4.4.1,* a SNR enhancement of 1.78 is achieved.

Figure 5.8 displays the effects of the pre-processing on a typical received signal, with the filtering stage removing low frequency noise and the stacking stage removing additional random interference, which occurs at frequencies within the passband. At each location examined, the application of the pre-processing results in one processed received

signal from each receiver and one processed *voltage output signal* for each central frequency and S-R separation.

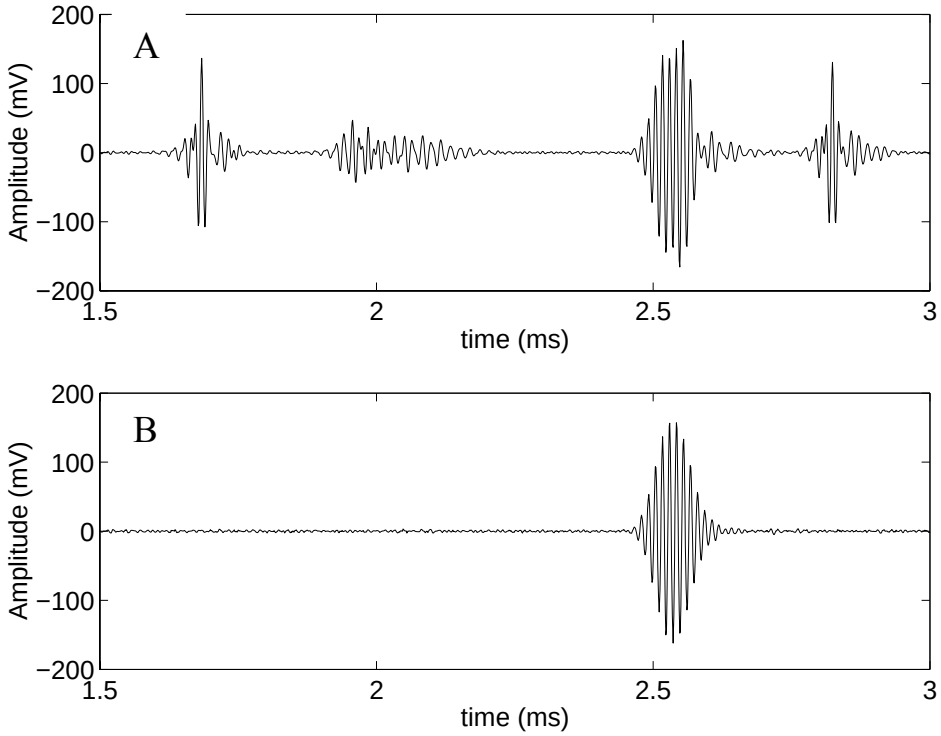

Figure 5.7. Comparison of mean (A) and median (B) stacks of typical received signal. Time axis has been limited to 1.5 to 3.0 ms to clearly display the effects in the vicinity of the directly transmitted pulse, which occurs between 2.5 and 2.6 ms.

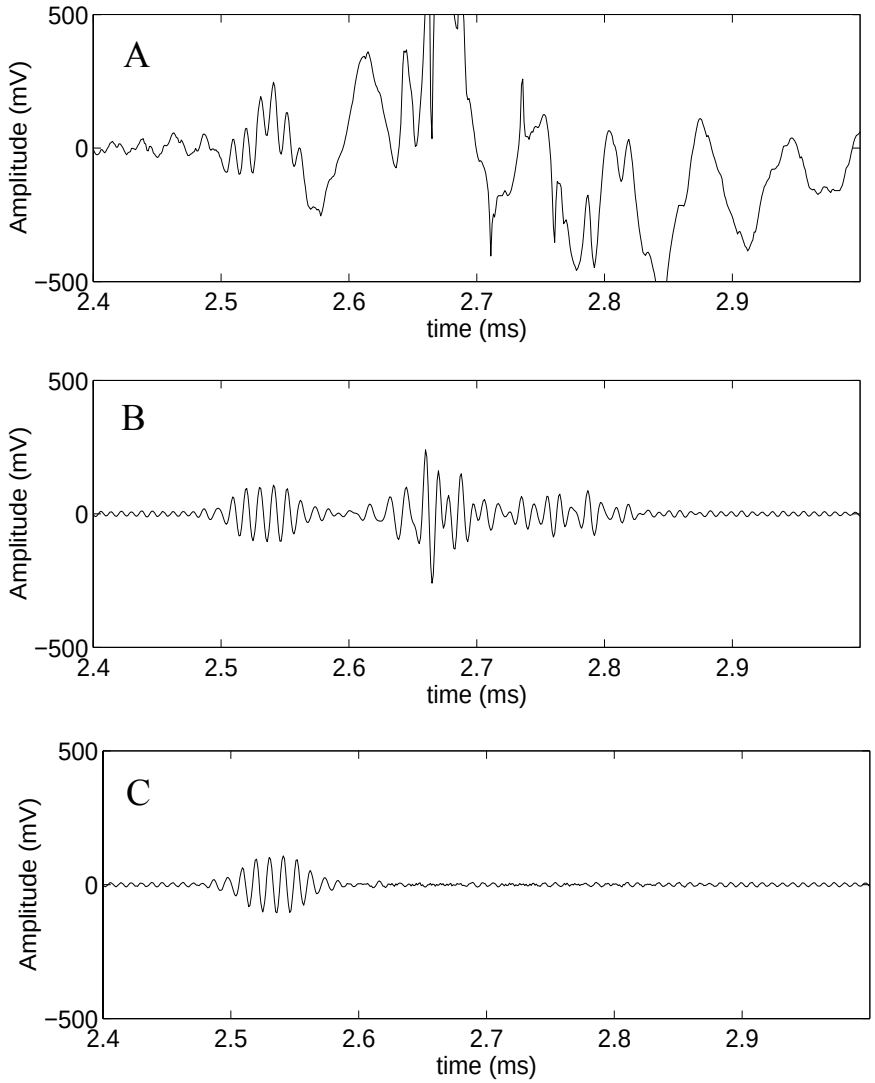

Figure 5.8. Example of pre-processing applied, including typical raw received signal (A), output of filtering stage for one received signal (B) and final output from median stack (C). Time axis has been limited to 2.4 to 3.0 ms, to display effects in the vicinity of the directly transmitted pulse, which arrives between 2.5 and 2.6 ms.

5.2. Calculation of velocity

The techniques developed to calculate the group velocity of the sediment optimise transmission data from a range of S-R separations. Knowledge of the delay times incurred by the electronic components of the device was not required and a thorough error analysis was undertaken.

5.2.1. Technique for velocity

The first step of the velocity calculation was to obtain the analytical signal of both the processed received signal and the corresponding processed *voltage output pulse*. The analytical signal $\xi(t)$ is a complex representation of the original signal,

$$\zeta(t) = x(t) + j\hat{x}(t) \qquad 5.8,$$

where $x(t)$ is the original signal and $\hat{x}(t)$ is the Hilbert transform. The Hilbert Transform is defined by the convolution of the original signal with the linear filter displayed in *Equation 5.9,* (Cohen, 1995),

$$\hat{x}(t) = x(t) * \frac{1}{\pi t} \qquad 5.9.$$

The analytic form of the signals possesses spectral amplitudes of zero for all negative frequencies and doubles the spectral amplitudes of the original signal for all positive frequencies.

The analytic form of the processed received signal was then correlated with the analytic form of the processed *voltage output pulse*. As displayed in *Figure 5.9A*, two events are observed in the received signal, the first corresponding to electronic cross-talk within the acquisition device and the second corresponding to the directly transmitted pulse. The resulting correlation function, *Figure 5.9B,* displays both these events, hence the period from 0 to 1.4 ms is zeroed in order to remove the correlation event corresponding to the cross-talk. As the earliest time at which the start of the directly transmitted wave was observed was 1.47 ms, this zeroing will not effect the direct transmitted pulse. The time t_R at which the remaining correlation function peaks is recorded.

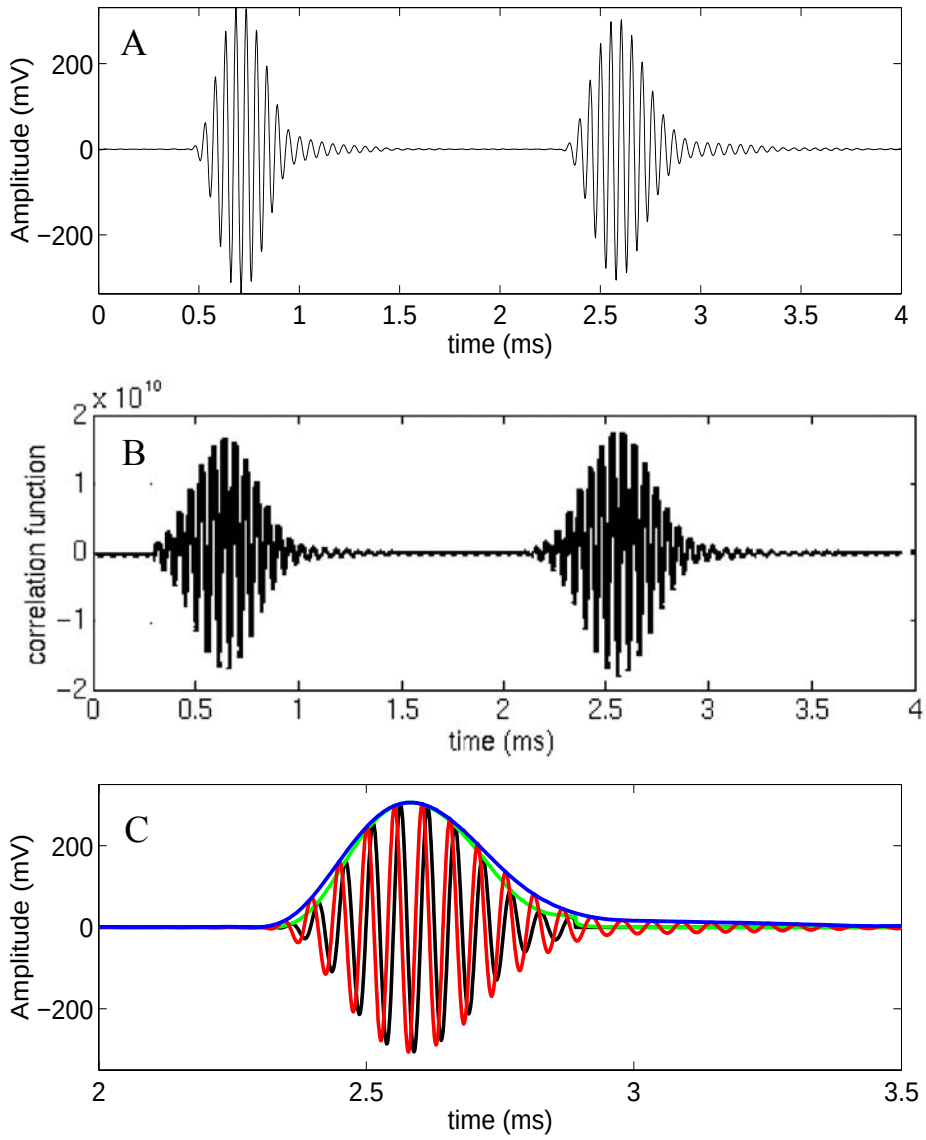

Figure 5.9. Example of correlation process used for a typical 20 kHz pulse, including a typical processed received signal (A), the resulting correlation function (B) and an overlay of directly transmitted pulse and shifted voltage output pulse (C). In C the received pulse is denoted by the red line, with a blue envelope, and shifted voltage output pulse is denoted by the black line, with a green envelope.

The cross-correlation of the analytical *voltage output pulse* was then calculated and the time t_V at which this peaked was recorded. The corresponding arrival time t_A was simply calculated from *Equation 5.10,* which will result in one arrival time for each central frequency and each receiver location examined,

$$t_A = t_R - t_V \qquad 5.10.$$

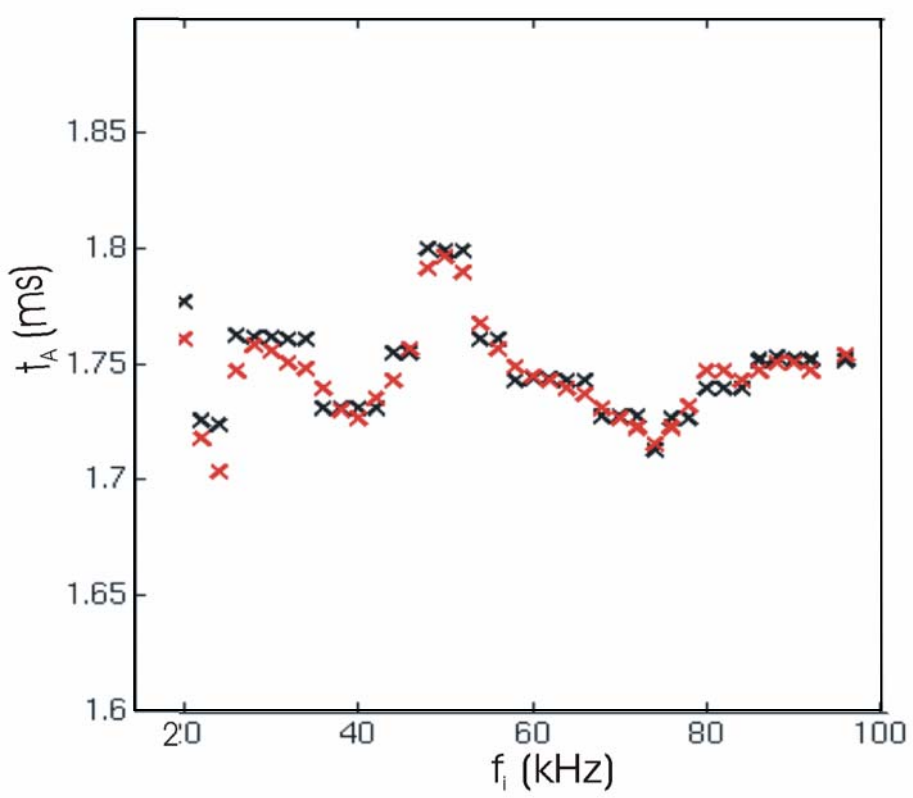

Figure 5.10. Comparison of arrival times obtained using original signals, black crosses, and analytical signals, red crosses.

The comparison of typical arrival times obtained using analytical signals to those obtained from the original signals is displayed in *Figure 5.10.* The use of the original signals results in discrete steps in the arrival times, which equal $\pm$ m·τ, where *m* is an integer and τ is the period of the dominant oscillation in the pulse. The arrival times obtained from the analytical signals produce more reliable arrival times, which vary in a smoother manner with frequency.

In order to calculate velocity at each location, the arrival times corresponding to each central frequency examined were considered separately. The arrival time obtained was equivalent to the sum of the time taken for the pulse to travel through the sediment t_S and an unknown lag time t_{lag}, which is introduced by the SPADE and acquisition device, *i.e.*

$$t_A = t_S + t_{lag} \qquad 5.11.$$

This lag time is the sum of the following delays:

- the time taken for the *voltage output pulse* to be transmitted from the output of the source amplifier to the source transducer;
- the time for the source transducer to transmit the acoustic pulse into the sediment, including that taken for the pulse to be transmitted through the polyurethane moulding surrounding the source transducer;
- the time taken for the directly transmitted acoustic pulse to be transmitted through the polyurethane moulding of the receiver transducer and be converted into a voltage signal;
- the time taken for this voltage signal to be amplified and stored by the acquisition device.

In order to account for these lag times *Equation 5.11* was re-expressed as

$$t_A = \frac{d}{v} - t_{lag} \qquad 5.12,$$

where d denotes S-R separation and v denotes group velocity. Hence arrival times were plotted against S-R separations for each central frequency used and a linear least-squares fit applied, an example of which is displayed in *Figure 5.11*. From *Equation 5.12*, it can be observed that the gradient of the fit is equal to the reciprocal of the velocity, while the lag time is equal to the intercept on the vertical axis. The velocity was therefore obtained from the reciprocal of the gradient of the line fitted to the plots of t_S versus d.

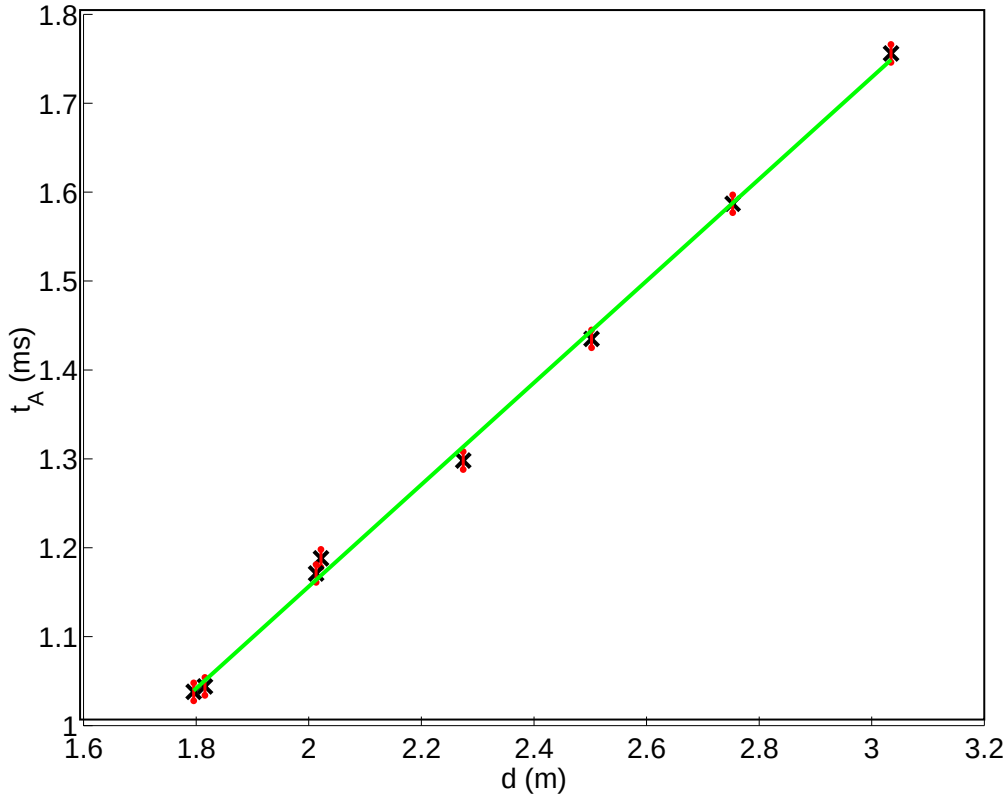

Figure 5.11. Example of linear fit applied at a central frequency of 50 kHz. Black crosses denote arrival times, with errors as red lines, while the green line displays linear least-square fit.

5.2.2. Justification of assumptions used in velocity calculation

A primary assumption in the velocity calculation is that the sediment volume through which the transmitted signals have propagated is homogeneous. The degree of sediment variability across this volume was assessed in *Section 4.4.3*, with mean grain diameter varying by less than 20 % at all locations examined barr one.

It is important to consider if a correlation between a processed received signal and processed *voltage output pulse* is valid. This is only strictly true if the source transducer and sediment do not alter the shape of the pulse, *i.e.* the received pulse resembles the *voltage output pulse* accurately. If this were the case, and the *voltage output pulse* was shifted by a time equal to the arrival time t_A, the peaks of the *voltage output pulse* and directly transmitted pulse would occur at exactly the same time. Such an overlay is displayed in *Figure 5.9.C* and though the envelopes of the two pulses peak at the same time, the peak of the shifted *voltage output pulse* actually lies 6 μs after the peak of the

received pulse. Hence the received pulse and *voltage output pulse* are not exact replicas of one another. The remainder of this section discusses the effect of pulse shape alterations on the processing techniques used to obtain group velocity.

For all frequencies, the discrepancies in the shape of the shifted *voltage output pulse* and received pulse detected in water are negligible, see *Section 4.2.3* for details. Typical received pulses that have been transmitted through sands (*i.e.* from the Studland 4, at a S-R of 2.33 m) are displayed in *Figure 5.12*. For all frequencies, differences in the shape of the received and shifted *voltage output pulses* are minimal, with the pulses exactly overlaying each other at 20 kHz. As typical pulses received in the silts are the same these are not displayed.

Hence, for saturated homogeneous sediment, the degree of distortion between the processed received pulse and processed *voltage output pulse* are minimal and much less than previously observed in the literature (Buckingham and Richardson, 2002). As *Section 3.2.4* outlines, the previous research recommends that a correlation between two received pulses is required to measure velocity accurately. However, the initial voltage pulse used by Buckingham possesses a square envelope, and hence sharp edges. This combines with the narrow-band nature of the source transducer to produce an acoustic pulse which is considerably distorted relative to the voltage pulse sent to the source transducer. The use of an untuned source transducer and a *voltage output pulse* with a smooth envelope in this project dramatically reduces the distortion and enables the use of a correlation between the voltage output pulse and the received signal. Any differences in the shape of the respective pulses will be incorporated by the error analysis discussed in *Section 5.2.3*.

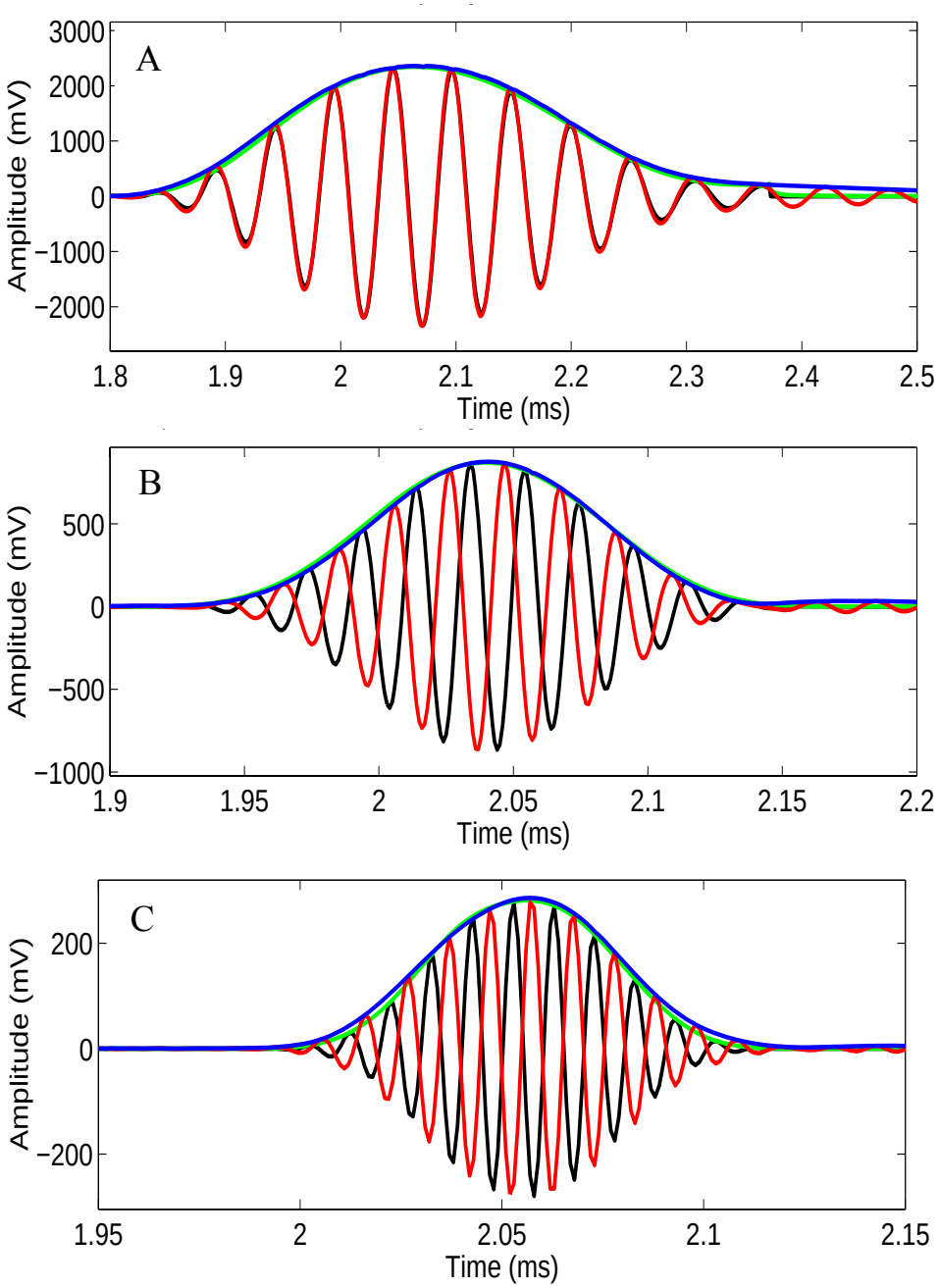

Figure 5.12. Typical pulses transmitted through a sandy sediment, i.e. Studland 4 at a S-R separation of 2.33 m. Pulses are displayed for central frequencies of 20 kHz (A), 50 (B) and 100 kHz (C). Note varying time axis to allow the fine details of the pulses to be displayed. The received pulse is denoted by the red line, with a blue envelope, and scaled and shifted voltage output pulse is denoted by the black line, with a green envelope.

It is interesting to consider the factors that can affect the reshaping of the pulse. These include:

1. The effects of the source and receiving transducers. The shape of the acoustic pulse emitted by the source and the voltage pulse generated by the receiver will depend on the central frequency of the pulse and the loading of the sediment (Buckingham and Richardson, 2002). Hence, for each location and central frequency examined, this will produce shape alterations which are the same for all S-R separation examined. This will produce the same "discrepancy" in the arrival time selected by the correlation approach used. This discrepancy will be incorporated in the lag of the linear fit applied and will not affect the resulting velocity.
2. The attenuation and dispersion effects of the sediment. The preferential attenuation of higher frequency components and variations in phase velocities of different frequencies are able to reshape the pulse. Though the use of a typical received wave as a reference wave would help to alleviate this problem, this would reduce the number of arrival times obtained at each frequency and so increase the resulting errors in the velocity obtained (see *Section 5.2.3*). An alternative approach is to model the reshaping of the pulse by the sediment (Jannsen *et al.*, 1985). This has been omitted as it assumes prior knowledge of the attenuation coefficient and velocity of the sediment and so can bias results.

The presence of heterogeneities in the sediment, *e.g.* shells, wood fragments and rubble will also modify the shape of the received pulse, through additional scattering of the pulse and additional arrivals. In extreme cases, the additional scattered or reflected arrivals can overlap with the directly transmitted wave, and so cause the received pulse to become unresolved (*Figure 5.13A)*. In some cases the power of the acoustic wave transmitted by the source was insufficient to allow the directly transmitted signal to be detected above background noise (*Figure 5.13B),* while in others the magnitude was too great and the received signal was clipped (*Figure 5.13C).* In all of the above cases the arrival times were neglected. However, in other cases, modifications to the received pulse were minor and the arrival times were retained, *e.g.* the received pulse was either just resolvable from additional arrivals (*Figure 5.13D)* or elongated with respect to the *voltage output pulse* (*Figure 5.13E*).

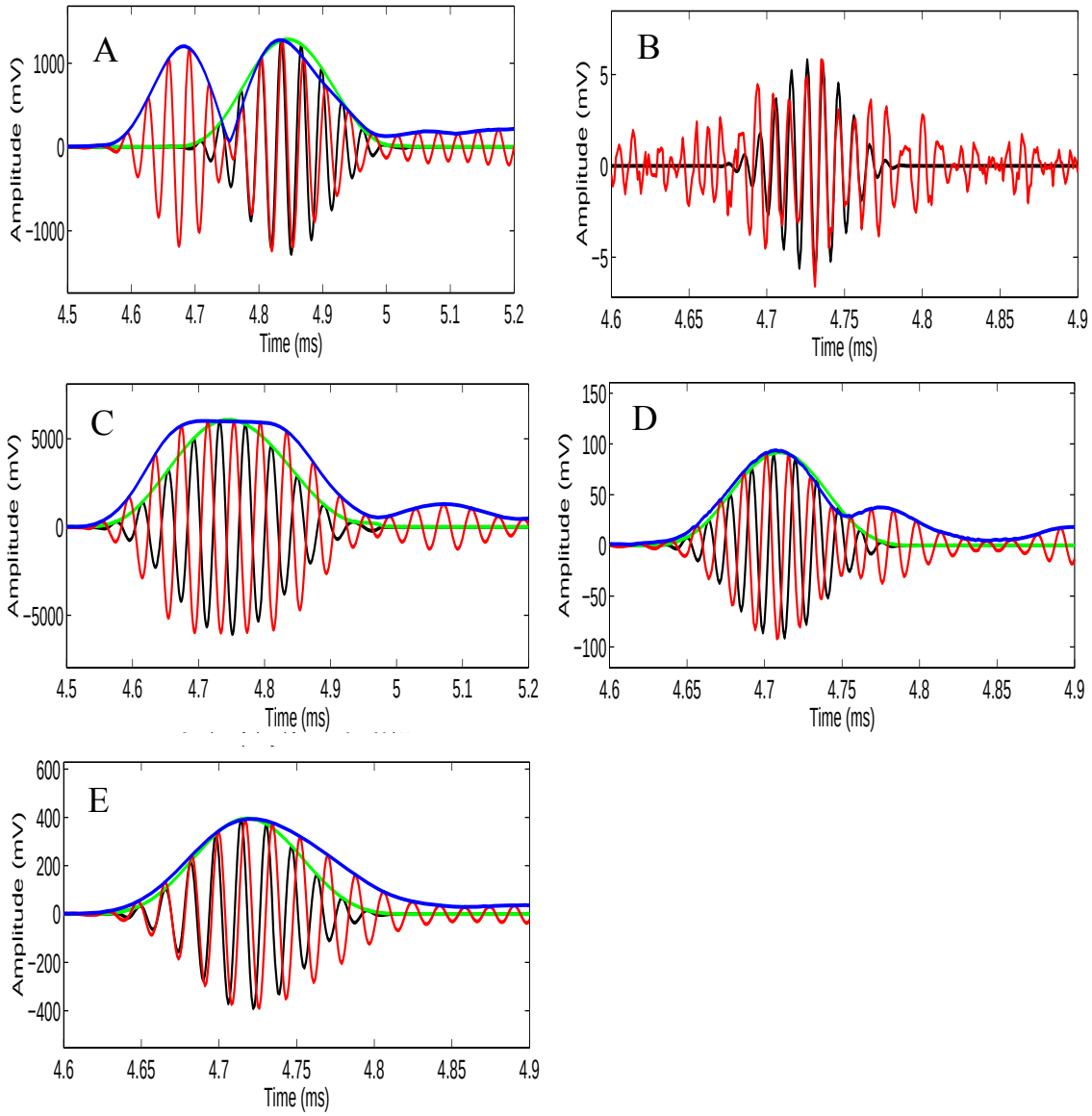

Figure 5.13. Examples of distorted received pulses (red lines with blue envelope) with scaled and shifted voltage output pulse (black line with green envelope) overlain to allow distortions to be observed: unresolved pulse (A), undetectable pulse (B), clipped pulse (C), "just" resolvable pulse (D) and elongated pulse (E). These are selected from the received signals at Needs Ore 3, with a S-R separation of 5.77 m. No envelopes are included in figure B as these cannot be clearly displayed for the undetectable signals.

5.2.3. Error analysis for velocity

The errors in the arrival time were obtained from two sources. The first was the intrinsic timing error dt_1 of the acquisition card used, which was accurate to $\pm$ 1 μs, *Section 4.2.3*. The second source arose from the cross correlation process, resulting in an

error denoted by dt_2. As discussed in *Section 5.2.2*, the arrival time selected does not correspond to the actual peak of the received wave. The time difference between the arrival time and the time at which the received pulse peaked was selected to quantify the resulting error. This was obtained for all frequencies, by examining received pulses from twelve different S-R separations, obtained from six different sandy locations and six different silty locations. The resulting time difference possessed a mean value of 10 μs, which is considered to be the relevant error in the correlation process. The total error of the arrival time DT was obtained by adding these errors in quadrature,

$$DT = \left(dt_1^{\,2} + dt_2^{\,2}\right)^{1/2} \qquad 5.13.$$

The standard deviation in the gradient of the linear fit applied σ_m was then calculated from *Equation 5.14,* from (Barlow, 1989).

$$\sigma_m = \left(\frac{DT^2.}{N_p(\overline{d^2} - \overline{d}^2)} \right)^{1/2} \qquad 5.14,$$

where N_p is the number of data points to which the linear fit is applied, d is the probe separation and the overscore notation denotes mean values. The standard deviation in the velocity σ_V is related to the standard deviation in the gradient through

$$\sigma_V = v \cdot \left(\frac{\sigma_m}{m_o} \right) \qquad 5.15,$$

where m_o is the gradient of the fit. The standard deviation in the estimated velocity is assumed to be equal to the relevant error in the velocity. For each location and frequency this will depend on the number of valid arrival times N_p that were used in the linear fit and the quality of the fit.

5.3. Calculation of attenuation coefficient

A specialised technique was developed to measure the effective attenuation coefficient of the sediment from transmission data from a range of S-R separations. This did not require knowledge of certain unknown parameters such as the TVR of the source transducer and the response of the receivers. The corresponding error analysis notably includes a quantitative examination of the repeatability of the coupling between the source and receivers and the sediment, a feature which has not been published in previous research.

5.3.1. Technique for attenuation coefficient

The first step in the calculation of the attenuation coefficient was to measure the amplitude of the received pulse. This was achieved by using the arrival times t_A to locate the *envelope* peak of the directly transmitted pulse (*Section 5.2.1)*. As the actual peak of the directly transmitted pulse deviated from this arrival time, the maximum peak-to-peak amplitude of the received signal lying between t_A-$2\tau_r$ and t_A+$2\tau_r$ was measured, where τ_r=$1/f_r$. An example of the region of received signal examined is displayed in *Figure 5.14.* To allow peak-to-peak voltages to produce reliable measurements, the selected portion of the received signal was interpolated to a sampling frequency of 10 MHz.

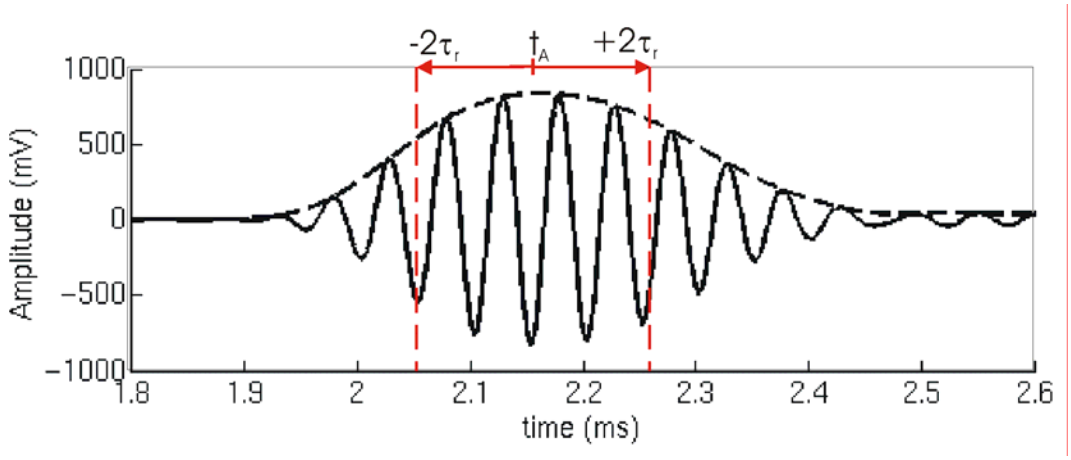

Figure 5.14. Example of region of received signal from which peak-to-peak amplitude is obtained.

The resulting amplitude *A(f,d)* is a result of the processes outlined in

$$A(f,d) = V_O(f) \cdot S_T(f) \cdot G(f,d) \cdot R_T(f) \cdot R_e(f) \cdot C \cdot e^{-\alpha_n(f)d} \qquad 5.16,$$

where spreading losses *G(f,d)* are a function of frequency and receiver location. The components which depend on frequency alone include the TVR of the source transducer $S_T(f)$, the response of the receivers $R_T(f)$, the electronic gain of the receiving amplifiers $R_e(f)$, the attenuation of the sediment in nepers·m^{-1} $\alpha_n(f)$ and the peak-to-peak voltage of the *voltage output pulse* $V_O(f)$. The coupling parameter *C* incorporates the coupling of both the source transducer and receivers to the sediment and is assumed to be constant at each location examined.

As the TVR of the source is unknown the technique developed must not require knowledge of this parameter. This is achieved by examining the received amplitudes at a range of S-R separations for each central frequency examined. For each individual central frequency the parameters $S_T(f)$, V_o and R_T are constant and *Equation 5.16* reduces to

$$A(d) = B_1 \cdot G \cdot R_e \cdot e^{-\alpha_n d} \qquad 5.17,$$

where B_1 now represents all terms which are considered to be constant at a fixed frequency and so amplitude now depends on S-R separation only.

The data to be compared at each frequency originates from two receivers with unique receiving amplifiers, which possess different electronic gains. Hence it was necessary to adjust the amplitudes from all receivers and frequencies to a constant gain of 60 dB. This is achieved by multiply the received amplitude by a factor of $10^{(60\text{-Re})/20}$, where R_e is the electronic gain of the corresponding amplifier in dB.

Spreading losses are calculated from the pressure fields predicted in *Section 4.3*.3. For each location examined the mean velocity across all required frequencies was obtained This approach is valid owing to the non-dispersive nature of the group velocities measured at the inter-tidal locations examined, see *Sections 6.1.1* and *6.1.2* for details. The pressure field which corresponded to the closest velocity and central frequency was then used, *e.g.* for a mean velocity of 1470 m·s^{-1} and f_r of 67.82 kHz the closest pressure field available was predicted for a velocity of 1500 m·s^{-1} and 68 kHz. Hence spreading losses can be accounted for by correcting the amplitude at a field-point *(y,z)* to that at the reference point by multiply by a factor of $10^{-\text{dB(y,z)}}$, where *dB(y,z)* is the required pressure at field-point *(y,z)* in dB relative to the reference point. While pressure fields could not be computed for all frequencies and velocities due to the large temporal demands of the simulation programme, the errors introduced by this discrepancy are incorporated through error analysis, *Section 5.3.2*.

This corrected amplitude, $A_C(d)$, is therefore obtained from *A(d)* using

$$A_C(d) = 10^{(60-R_e)/20} \cdot 10^{-dB(y,z)} \cdot A(d) = B_2 e^{-\alpha_n d} \qquad 5.18,$$

where B_2 represents the new constant.

Taking natural logarithms of *Equation 5.18* results in

$$\ln(A_C) = \ln(B_2) - \alpha_n d \qquad 5.19.$$

Hence, at each location and frequency, the natural logarithm of the corrected amplitude was plotted against S-R separation and a weighted linear least-squares fit applied (Barlow, 1989). *Figure 5.15* displays the application of a typical linear fit. As in the case of velocity amplitudes from distorted received pulses were omitted from the analysis, see *Figure 5.13*. The magnitude of the gradient of this fit equals the attenuation of the sediment in nepers·m^{-1} and is converted into dB·m^{-1} using

$$\alpha = 8.686 \cdot \alpha_n \qquad 5.20,$$

where α is attenuation in dB·m^{-1}.

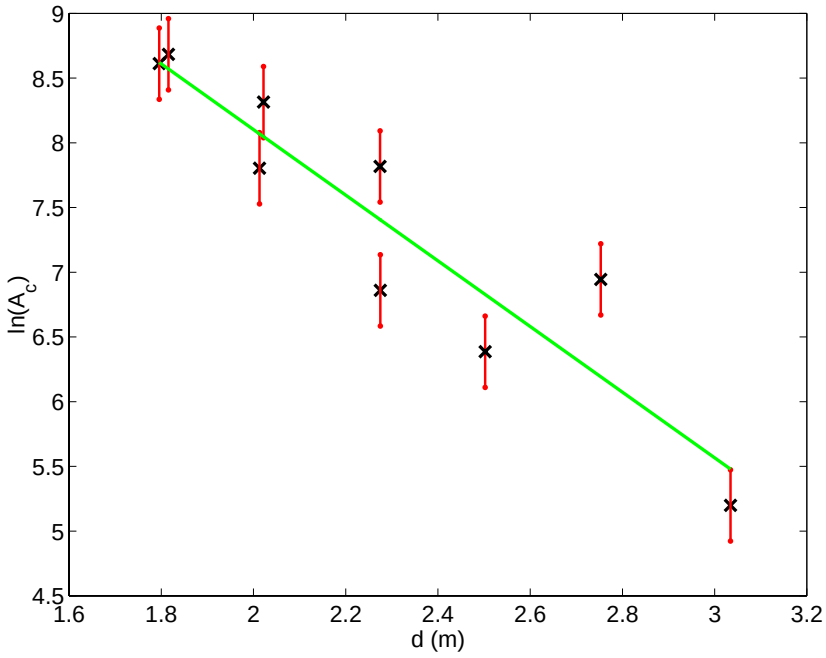

Figure 5.15. Example of linear fit (green line) used to obtain attenuation, with black crosses denoting corrected amplitudes and errors displayed as red lines.

5.3.2. Justification of assumptions used in attenuation calculation

As in the technique developed to measure velocity, it is assumed that the sediment examined at each location investigated is homogeneous, see *Section 5.2.2* for details.

Two additional assumptions are made in the construction of *Equation 5.17*. Firstly, it is assumed that the peak-to-peak voltage of the *voltage output pulse* V_O is constant for each location and central frequency. As standard deviation in the mean voltage of the *voltage output pulse* is less than 5 % at each central frequency (*Section 4.*2), the variability

in the peak-to-peak voltages will be less than 5 %. The introduction of a "coupling" variability term later in this section will accommodate these variations.

Secondly, it is assumed that the coupling parameter C is constant at each location across all deployments and central frequencies. The coupling of the source and receiver transducers to the marine sediment will affect the amplitude of the acoustic wave emitted into and detected from the sediment. While previous workers have identified variable coupling between probe deployments as a considerable source of error, no quantitative assessments of this error have been published, *Section 3.2.*

The repeatability of the coupling was determined as follows. Rearrangment of *Equation 5.16* for each location and frequency gives

$$C = \frac{A(d)}{B_3 \cdot R_e \cdot G(d) \cdot e^{-\alpha_n d}} \qquad 5.21,$$

where B_3 now incorporates the effects of the voltage output pulse V_o, the TVR of the source transducer $S_T(f)$ and the response of the receiving transducers R_T, all of which are constant. Amplitudes were corrected for receiver electronic gain and spreading losses, as described in *Section 5.3.2*. Finally, the amplitudes were conditioned to account for the attenuation of the sediment between the reference point (1 m from the source along the zero degree line) and field-points at which the receivers were deployed. This was achieved by multiplying by a factor of $e^{-\alpha_n (d-1)}$, where α_n is the previously calculated attenuation coefficient in nepers·m^{-1} at the relevant location and frequency. Hence *Equation 5.21* can be re-expressed as

$$C = \frac{A_{CO}(d)}{B_3} \qquad 5.22,$$

where $A_{CO}(d)$ is the conditioned amplitude which is obtained from $A(d)$ using

$$A_{CO} = A(d) \cdot e^{-\alpha_n (d-1)} \cdot 10^{\frac{(60-R_e)}{20}} \cdot 10^{-dB(y,z)} \qquad 5.23.$$

This procedure effectively transforms amplitudes measured using different receivers at different field points to corresponding value for a single point (the reference point) and receiver. To examine the effects of variable coupling between deployments on received amplitudes, only locations which possessed usable data from at least five deployments of receiver pairs and at which no evidence of heterogeneities were observed are used. The selected locations are given in *Figure 5.16.* For each location, conditioned

amplitudes were calculated, and the mean percentage error associated with coupling variability *%CE* was calculated for each central frequency using

$$\%CE = 100.\frac{std(A_{CO})}{mean(A_{CO})} \qquad 5.24,$$

where $mean(A_{CO})$ and $std(A_{CO})$ are the mean and standard deviation of the conditioned amplitudes respectively. Though the main factor responsible for the variability term computed from *Equation 5.24* is the coupling between the sediment and the probes, the following additional factors will provide lesser contributions:

- A small degree of sediment heterogeneity is observed at all locations examined, with even the most homogeneous location displaying a variability of 1.38 % in mean grain diameter, *Section 4.4.3*. This will introduce variability through the correction for sediment attenuation and spreading losses.
- Variations in the peak-to-peak amplitude of the *voltage output pulse*, which are less than $\pm$ 5 %.
- Errors in the relative positions of the source and receivers. The errors which have the most pronounced effects are $\pm 2^{o}$ in the inclination of the probes to the vertical and $\pm$ 0.02 m in the relative depth of the probes (see *Section 4.4.1*). These errors are transmitted to the received amplitudes through the correction for spreading losses and the receiver beam response, with maximum predicted errors occurring at the highest central frequency and smallest S-R separation examined. For this worst-case scenario, corrections for spreading losses can allow received amplitudes to be overestimated by up to 5.6 dB, while the effect of the receiver beam pattern may allow received amplitude to be overestimated by up to 6 dB. This highlights a disadvantage of using large transducers, with smaller transducers producing less focused beams.

The percentage error in amplitude associated with coupling variability range from $\pm$ 0.3 to $\pm$ 60.6 %, with a mean value of 27.4 % and no frequency-dependent trends observable, *Figure 5.16*. The reduced number of data points at frequencies less than 30 kHz is a consequence of wave interference preventing the required attenuation coefficients from being obtained for these frequencies at certain locations (see *Section 6* for details).

Though the "coupling" variability is significantly large, the use of the attenuation calculation described in *Section 5.3.1* is justified through the lack of a frequency-dependence in the percentage error observed. This implies that variations in the coupling

parameter are also random and hence the application of a linear fit, *Figure 5.15,* to amplitudes obtained from a number of deployments will reduce the effects of the variable coupling. The use of a percentage errors in amplitude of $\pm$ 27.4 % in *Section 5.2.3* will accommodate errors from variable coupling, sediment heterogeneities, variations in V_o and errors in probe positions.

It is difficult to quantitatively assess the degree to which previous measurements of attenuation coefficient obtained from *in situ* probes have been affected by coupling variability, as the degree of variability is dependent on the manner in which probes were deployed, the sediment under examination and the dimensions of the active faces of the probes. However, the repeatability of coupling theoretically increases with the surface area of the active faces of the probes. As the SPADE source and receivers possess surface areas much greater than those published for alternative *in situ* devices, it is postulated that previous work has suffered from variations in coupling which are greater than 27.4 %.

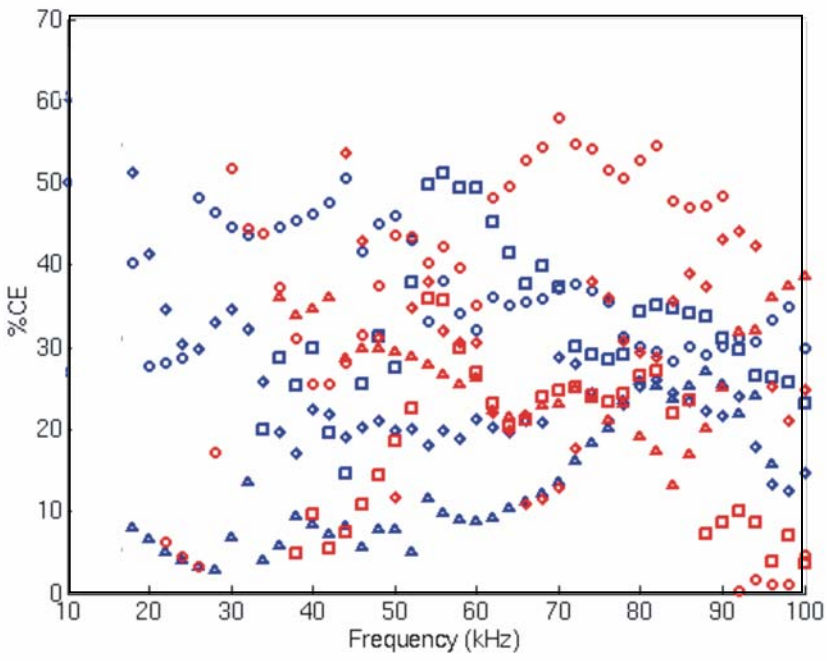

Figure 5.16. Percentage error due to coupling variability %CE from eight locations examined which possessed a suitable range of usable S-R separations and no visual evidence of heterogeneities. Locations examined include: Studland 4 (blue circles), Branksome 1 (blue squares), Lilliput 1 (blue diamonds), Lilliput 4 (blue triangles), needs 1 (red circles), Needs Ore 3 (red squares), Universe 1 (red diamonds) and Universe 2 (red triangles).

5.3.3. Error analysis for attenuation coefficient

The error analysis for attenuation coefficient was more complex than for the case of velocity. Errors in the amplitude of the received signal arose from several sources, which included:

- *Type 1 errors.* These correspond to the intrinsic sampling errors of the acquisition card used, which were measured to be $\pm$ 2.5 mV. As the signals analysed are a median stack, the resulting error dA_1 is obtained from

$$dA_1 = \pm 2.5 \cdot \sqrt{\pi / 2N_S} \qquad 5.25,$$

where N_S is the number of shots (Cramer, 1946) and $dA_1 = \pm 1.4$ mV for five shots.

- *Type 2 errors.* These arise from the variability in the coupling parameter and are equivent to $\pm$ 27.4 % of each amplitude.

- *Type 3 errors.* These result from the from uncertainty in the gain of the receiving amplifiers. This introduces an error of $\pm$ 0.224 dB in A_C.

- *Types 4 errors.* The use of spreading losses which may correspond to a velocity which differs from the observed velocity in the sediment by a maximum value of $\pm$ 50m·s^1 introduce errors into the corrected amplitude. In order to calculate these errors, the difference between the two predicted pressure fields that span the velocity of the site was calculated for each frequency and field-point, an example of which is displayed in *Figure 5.17.* The error in the spreading at a field-point *(y,z)* was then taken as half the difference at this field-point. These were less than $\pm$ 0.1 dB for all required velocities and frequencies, a consequence of the required field-points all lying in the far-field where variations.

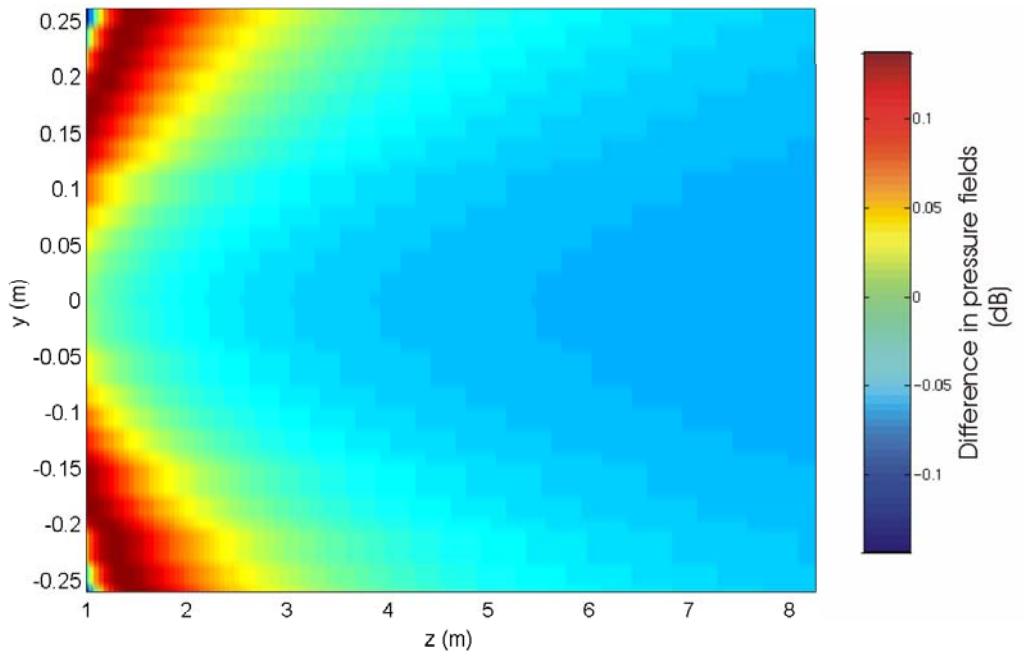

Figure 5.17. Difference between predicted fields with velocities of 1700 and 1800 m·s^{-1} at 50 kHz.

For convenience, the errors measured in dB (*Type 3* and *4 errors*) were combined first by transferring the errors through the correction process used to account for spreading losses and receiver gain. The resulting error was then combined in quadrature with *Type 1* and *2 errors* to obtain a final error in the corrected amplitude A_e. As the amplitudes used in the calculation of attenuation coefficient ranged from 5.7 mV to 10 V, either *Type 1* or *2* errors represent the dominant component, with errors from *Type 3* or *4* resulting in percentage errors in amplitude less than 2.6 % and 1.0 % respectively. The error in $ln(A_C)$, which is denoted by $\Delta\{ln(A_C)\}$ is simply equal to A_e/A_C (Barlow, 1989). To obtain the standard deviation in the attenuation coefficient, σ_α, these were combined with the error in the probe separation d using a weighted linear least-squares fit

$$\sigma_\alpha = 8.686 \cdot \left(\frac{\overline{\overline{\Delta\{\ln(A_C)\}^2}}}{N_p\left(\overline{\overline{d^2}} - \overline{\overline{d}}^2\right)} \right)^{1/2} \qquad 5.26,$$

where double overscore denotes a weighted mean and N_p is the number of datapoints to which the linear fit is applied. The use of weighted means accounts for the variable errors in $ln(A_C)$. An example of such a weighted mean for S-R separation d is

$$\bar{\bar{d}} = \frac{\sum_{1}^{N_p} d_i / \Delta d_i^2}{\sum_{1}^{N_p} 1 / \Delta d_i^2} \qquad 5.27,$$

where d_i is the *ith* value of d and Δd_i the corresponding error ($\pm$ 1 cm).

5.4. Calculation and error analysis of quality factor

The quality factor Q of the sediment was calculated from the approximation equation discussed in *Section 2.1, i.e.*

$$Q = \frac{\pi \cdot f_r}{\alpha_n \cdot v} \qquad 5.28,$$

which is valid for quality factors greater than 10. The standard deviation in Q, which is denoted by σ_Q, obtained from the quadrature addition of the standard deviation in the group velocity and the effective attenuation coefficient,

$$\frac{\sigma_Q}{Q} = \left(\left[\frac{\sigma_\alpha}{\alpha} \right]^2 + \left[\frac{\sigma_V}{v} \right]^2 \right)^{1/2} \qquad 5.29.$$

5.5. Summary

The processing techniques developed within this section to obtain the group velocity, effective attenuation coefficient and quality factor include a number of factors that have not been presented by previous researchers. The velocity technique does not require knowledge of unknown lag times introduced by the device, while the use of a correlation between the received pulse and *voltage output pulse* is justified though an examination of the pulse envelopes and a detailed error analysis. The technique for calculating attenuation coefficient incorporates spreading losses which are directly relevant to the sediment under examination and introduces a quantitative assessment of the variability in the received signal. This pre-dominantly arises from variability in the coupling between the probes and the sediment, with additional contributions from the variability in the *voltage output pulse*, sediment heterogeneities and uncertainties in the relative positions of the source and receivers. These factors introduce a mean variability of 27.4 % in the amplitude of the received pulse, which is incorporated into the corresponding error analysis.